A Research Method for Shock Loadings on Rotation Isolator used in Course Correcting Fuse

Jianghai Hui, Min Gao, Yi Wang, Cheng Cheng

***Abstract*—This paper proposes a simulation method in order to analyze the dynamic response of the components in ammunition to the sever shock loadings during the process of launch accurately It is the implicit-explicit sequential finite element dynamic analysis to research the shock loadings on the rotation isolator used in Course Correcting Fuse. The paper builds an integrated model containing isolator, projectile, gun tube and breech. The simulation process is finished by mesh generation, setting the loads boundary conditions, contact definition and output control. At first, gun tube's deformation due to gravity at 52 degrees quadrant elevation was acquired from the implicit analysis. Then the displacement and velocity of projectile are obtained to verify the gun tube's deformation through the explicit analysis. The bearings' axial and transverse acceleration in the isolator are depicted. The results of the research indicate that the gun tube deformation, base pressure and pressure dissipation at the muzzle exit are main factors to influence the shock loadings on the isolator. The projectile's accelerated spin and the collision with the barrel inside wall produce centrifugal inertia force and gyroscopic couple which influence the transverse shock loadings. In addition to this, a calculation method is proposed to work out the maximum contact stress of the bearing's components. The method is combined with the bearings' components maximal contact stress in the process of simulation. The results of the research prove that the calculation method is correct and credible. The research conclusions provide some reference for the structural design of Course Correcting Fuse.**

***Index Terms*—rotation isolator, implicit-explicit sequential finite element analysis, shock loadings, bearing**

I. Introduction

Smart artillery munitions, equipped with guidance and control system, which contain kinds of sophisticated embedded electronic system and electric actuating mechanism such as machine and canard, have been developed by the US Army during the last forty years. In 2006, the operating theory of Precision Guidance Kit showed in Fig.1 was firstly introduced by United States in their patent, two-dimension guidance of projectile fixed wings. In this paper, the Course Correcting Fuse, belongs to a kind of Precision Guidance Kit is regarded as the study object. The electricity devices in the fuse which is powered by power source control the spin of the fixed wings tied to the fuse. Therefore, it can change the aerodynamic characteristics of the projectile and make precision guidance for uncontrolled projectile come true. The fuse screws to the projectile through the rotation isolator, therefore, rotational movement relative to projectile can be realized by it. In gun-launched projectiles, large shock loadings both in axis and transverse direction generated during a launch process tend to cause the sophisticated devices to fail. It is the reason to improve the operating performance, accurate identifications for stress circumstance during then launch and reduction of the shock loadings applied to the components in the fuse are the critical issue must be taken into account.

Fig. 1. Precision Guidance Kit

It is a complex dynamic process that the projectile pushed by the gas at high pressure from the propellant moves from the breech to the muzzle of the gun barrel with high speed rotation accelerated to 18000 rpm at the muzzle exit by interaction of rifling and band. The shock loadings applied to the system, and devices are difficult to be measured and the dynamic response to shock cannot be analyzed accurately.

Earlier in the study, the researchers developed the model in a simple way and conducted simplified experiments to analyze the dynamic process during projectile launch. Simkins et al. predicted resonant condition of the projectile and gun tube through dynamic experimental analysis [1]. A two-dimensional quasi-static model of a training projectile was developed by Hollis and with this model the projectile was redesigned to reduce stresses [2]. Hopkins and Wilkerson

This work is supported by National Deference Pre-Research Foundation of China.

Jianghai Hui is with Shijiazhuang Mechanical Engineering College, No.97 Heping West Road, Shijiazhuang, Hebei, 050003, China (corresponding author to provide phone: 18330170253; e-mail: huijh001@163.com).

Min Gao is with Shijiazhuang Mechanical Engineering College, No.97 Heping West Road, Shijiazhuang, Hebei, 050003, China (e-mail: gaomin1103@gmail.com).

Yi Wang is with the Shijiazhuang Mechanical Engineering College, No.97 Heping West Road, Shijiazhuang, Hebei, 050003, China (e-mail: wamgyi050926@163.com).

Cheng Cheng is with the Shijiazhuang Mechanical Engineering College, No.97 Heping West Road, Shijiazhuang, Hebei, 050003, China (e-mail: clarence_oec@sina.com).

developed an axisymmetric transient FEM of the M256 gun system to explain the experimental results on reducing the dynamic motion during firing [3].

As research continued, experimental test is too expensive and time-consuming to conduct and there are some uncontrollable factors during test leading to failure of demonstrating theoretical and experiential analysis. However, the researchers in this field gradually adopted numerical models such as finite-element models like the flight vehicle [4], [5]. Engineers and researchers in US Army performed static and quasi-static analysis in centrifuge tests with the use of pressure-time curves and peak acceleration value to design the components and improve their overloading-resistibility [6]. They once conducted three types of tests to find failures and build reliability of Systems, subsystems, and components in projectile [24]. Kessler and Spearing designed and tested the aft section of a kind of autonomous flying vehicle which was subjected to high impulsive inertial loads by developing a quasi-dynamic FEM of the aft section [7]. Chowdhury et al. conducted the parameters study in identifying sensitive factors affecting the muzzle exit dynamics of projectile with an integrity model including balloting, spinning and gun mount position. Then they determined the resulting vibrations of a projectile through developing a 3D explicit dynamic finite element model [8]. Petersen et al. developed the FEM and conducted the simulation by SIMBAD and Abaqus to compare with experimental data, including position, acceleration, and strain of a projectile during firing to improve correlation between dynamics modeling and test data. [9]. To better understand how shocks send to electronic boards and ways to mitigate shocks, Chakka et al. created a 3D FEM and illustrated the dynamic response of the devices in the projectile. [10]. Tzeng et al. regarded the rail gun as a beam with an elastic foundation, and they created a transient 4th differential equation based on the result data from the analysis of dynamic behavior during launching to describe the structure response of the gun. However, they neglected the flexibility of the gun. [11]. Laughlin analyzed the dynamic behavior of a gun-launched projectile through a 3D explicit FEM and studied the effect of geometry on the intensity of transverse acceleration caused the electronic components failure. [12]. Somasundaram created a projectile model which could mimic an actual projectile to study the effect of the tightening preload torque on accelerations and frequencies of components on boards [13]. Reinhardt et al. found that there was a significant reduction in accuracy when solder is not included in the model developed with finite element method [14]. With explicit axisymmetric Lagrangian-Eulerian Finite Element simulation adopted, Yin et al. obtained the dynamic characteristics of the precision-guided projectiles during launch process and investigated the whole process of firing to observe the local and global feature of setback, set forward pressure and acceleration histories [15]. The results indicated and described the effects of different media including the propellant, projectile, confined volume and free space. Kuncham from University of Nevada presents the effect of shock and the structural response of the electronic components within the projectile and results are verified by experimental and modal analysis [23].

Based on the response of devices with in the projectile and the interaction between the gun tube and projectile during launch, it is also important to find schemes to reduce the shocks on them. Cui, et al. analyzed the anti-shock performance of the electronic devices in the electromagnetic launched projectile with establishing a mathematical model of the two-phase pulsed alternator. They also used the finite analysis software to create finite element model including printed circuit and other components [21]. With adopting optimization algorithm, some researchers obtained the optimum parameter design about performance indexes [16]. The electronic devices always failed due to shocks during launch. With the theory of wavelet and the means of FEA, Heaslip and Punch reduced the failure of devices in projectile with foam materials. However, this method may affect the upgrade and replacement for the system. [6]. Chakka et al. used carbon fibers embedded in an epoxy matrix and studied the effect of reducing the transmitted shocks during launch with the composite supporting plate by varying the thickness of it. [10]. Somasundaram adopted stiffeners and dampers to protect electronic devices in the projectile. However, when the frequency of acceleration exceeds 5,000 Hz, they discovered that it cannot protect the electronic devices [13]. Sueki et al. created finite element model of a layered cylindrical structure and simulated to verify that the effect of impedance mismatch in axial acceleration response under shock loadings [17]. Researchers tend to acquire the correct results with using precise model, which also have good agreement with actual situation. However, aiming at most complexity of problems, researchers and engineers oversimplified the model of projectile and its devices or components. A report of process Excalibur and SADARM smart projectiles presented that the models in design are too simplified to get the dynamic response accurately. In addition, the oversimplified models generat the failures of devices in the projectile during verification testing [10], [18]. Engineers researched for traditional existing models based on quasi-static conditions, thus using the results from the models to correct boundary conditions [4], [5]. The reasons for the failure of onboard-embedded electronic cannot be accurately predicted by the quasi-static analysis are following illustrated:

First, most structures fail after moving out of the muzzle. However, many researchers always ignore the effect of shock loadings at the muzzle exit, and it is too complex for them to analyze. Second, researchers are likely to neglect transverse shock loadings, which generate the high-frequency vibrations of structure and cause failure [5], [10], [14], [18].

In addition, the sudden decrease in loading resulted from the gas expand freely at the muzzle exit caused the oscillation of the projectile at high frequencies around its center of gravity [4], [18]. And researchers always ignore the nonlinear transient conditions resulted from the interaction between the gas and projectile [19]. Reference [15] examined that the reflected waves as well as spring back of the precision-guided projectiles resulted from these local oscillations as it moves out of the muzzle. Numerous failures of sensitive equipment within the munitions programs like the US Army's Excalibur and SADARM were experienced due to shock from muzzle exit transient. The shocks transmitted to the embedded electronic system resulted in the great possibility of failure rather than the maximum axial acceleration. The transverse

movement of the projectile is no longer constrained by the barrel wall, so it was not allowed to neglect the balloting acceleration in the set forward region [20]. Besides, US Army Researchers developed deterministic barrel model that possesses both vertical and lateral deviations from centerline in accordance with measurement data, and simulated comprehensive barrel centerline variations for the investigation of projectile balloting motions by a novel approach [22].

This paper conducts the implicit-explicit sequential finite-element analysis in order to research dynamic response of the rotation isolator used in the Course Correcting Fuse to the shock loadings during launch. At first, we create an integrated model containing gun tube, breech, projectile and the isolator in the Course Correcting Fuse. Then, the pre-processing, including modeling, element type, material, mesh, boundary condition, solution controlling will be described. Next, the dynamic response of the bearings in the isolator to shock loadings will be analyzed. Finally, we calculated the maximum contact stress of the important components in the fuse through Hertz theory.

The remainder of this paper is organized as follows: Sect.2 presents the description of the integrated model, including gun tube, breech, projectile and rotation isolator in the Course Correcting Fuse. Sect.3 describes the pre-processing of simulation. Sect.4 reports the simulation results that address the characteristics of dynamic response of the bearings in isolator to the axial and transverse shocks, and proposes the calculation method combined with the simulating in previous section to work out the maximum contact stress of bearings in based on Hertz theory. In sect.5, we conclude the paper.

II. Model Desription

It can be seen from Fig.2 shows that the Course Correcting Fuse is screwed onto the projectile. Inside the rotation isolator, there is a permanent magnet machine served as a power source, while it is also used to drive and control relative rotation between the fixed canard and projectile. Rotation isolator is comprised of bearings, housing and shaft, which was simplified by eliminating exact details in modeling. The fixed canard mentioned above is screwed onto the shaft and electricity components occupying inside fuse were simplified as the payload. There are three bearings, two deep groove ball bearings (hereinafter referred to as the ball bearing) and one axial needle roller thrust bearing (hereinafter referred to as the thrust bearing), inside the isolator connecting the housing and shaft to realize the relative rotation between projectile and canard. The projectile and fuse are subjected to axial and transverse shock loadings exceed 15,000 G's during artillery firing within a few milliseconds. Plastic deformation or cracks on the contacting surfaces between raceway grooves and rollers occurred under shock loadings, locating the cause that failure of the fuse during flight.

Based on the description above, the structure of isolator is designed as Fig.3 shows. The thrust bearing is adopted to improve the capacity of shock resistant for isolator. It can experience the majority of shock loadings thus preventing the two ball bearings from plastic deformation or cracks. According to manual data, the rated static load of the thrust bearing is about 20,000 N. To ensure operating reliability during launch and decrease the adverse effect on the isolator and other devices, the buffers are added between the thrust bearing and the housing to isolate the shock loadings produced by the propellant explosion. The influence of the canard and electronic components cannot be neglected, so a 1.3-pound mass payload was attached to the shaft.

As mentioned in sect.1, the transverse acceleration should not be neglected. The manufacturing imperfections and gas leakage between the projectile and gun barrel cause the projectile to be subjected to transverse shock loadings, known as balloting, inducing continual violent impacts with the barrel's inside wall. Balloting is the transverse motion of a projectile inside a gun tube during launch and is affected by the parameters such as CG position, band location, projectile length, wheel base length and tube bending. The first four determined by manufacturing cannot be analyzed in research, while the tube bending can be simulated in the gravity field by implicit analysis. Above all, gun tube and projectile will be modeled and simulated by the scheme of implicit-explicit sequential finite-element analysis.

Besides the gun tube and breech, the projectile, comprised of hollow steel shell, charge and band was modeled as Fig.4. shows.

III. Development of FEM

A. Material Properties

The properties for each part of model are listed in TABLE I

B. Mesh

SOLID185 is used for 3-D modeling of solid structures. It is defined by eight nodes having three degrees of freedom at each node: translations in the nodal x, y, and z directions. The geometry and node locations for this element are shown in Fig.5. It allows for prism and tetrahedral degenerations when used in irregular regions.

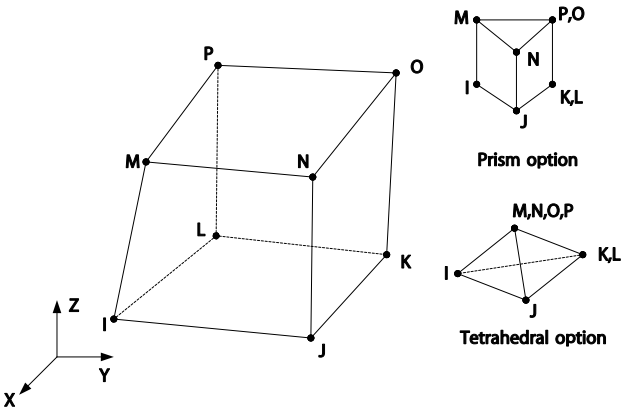

Fig. 5. SOLID185 Geometry

SOLID164 is used for the 3-D modeling of solid structures. The element is defined by eight nodes having the following degrees of freedom at each node: translations, velocities, and accelerations in the nodal x, y, and z directions. The geometry and node locations for this element are shown in Fig.6. This element is used in explicit dynamic analyses only. It allows for wedge, tetrahedral and pyramid degenerations when used in irregular regions.

The model was meshed by creating a three-dimensional solid for each part with quadrilateral element used. For implicit simulation, each part of model was given implicit

element type SOLID185 while the explicit element type SOLID164 transferred from SOLID185 was used in explicit analysis.

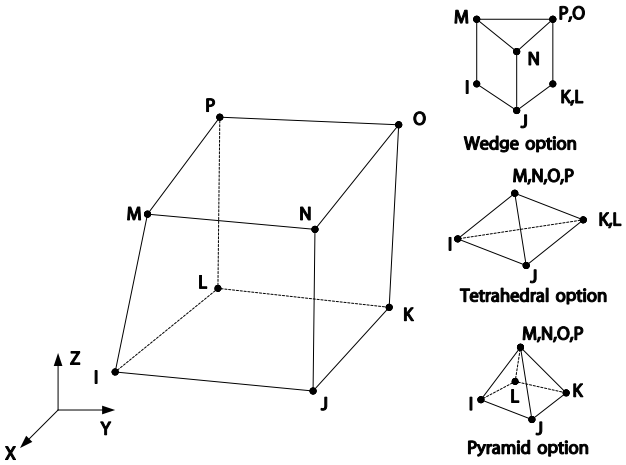

Fig. 6. SOLID164 Geometry

C. *Loads and boundary conditions*

Static analysis is conducted under the displacement boundary conditions in order to gain the deformation of the gun tube due to gravity. Firstly, like cantilever beam, the gun tube was fastened with the breech prevented from translating and rotating in any direction. So the boundary condition, as Fig.7 shows, was given 0 to the displacement of breech and base of the gun tube in the x, y and z directions.

Secondly, the gun tube is elevated to 52 degrees QE during launch, so another condition was needed to keep the projectile from moving due to gravity in the z and y directions, but to leave it free to move in the x direction. In addition, the gravity is applied to the whole model in the z (-7.723 m/s^2) and y (6.033 m/s^2) direction.

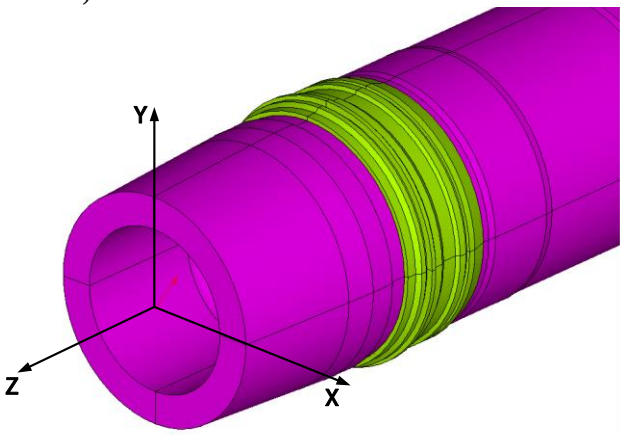

Fig. 7 Local coordinate system on projectile

The chart (a) of Fig.8 shows a typical pressure-time curve. The changing curve of chart (b), the base acceleration time history is transformed from p-t curve according to Newton's Laws. Then the base acceleration is regarded as the axial loading condition. It is applied to the base of the projectile.

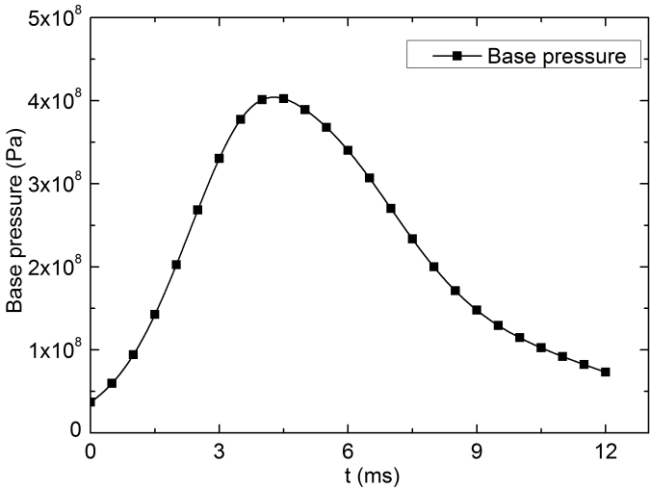

(a) Base pressure

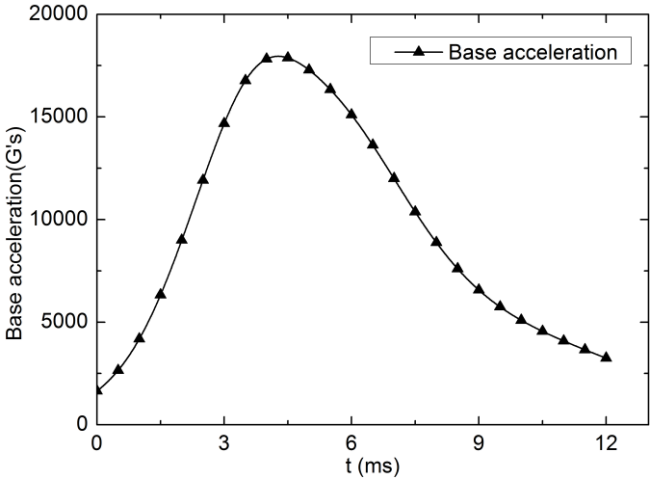

(b) Base acceleration

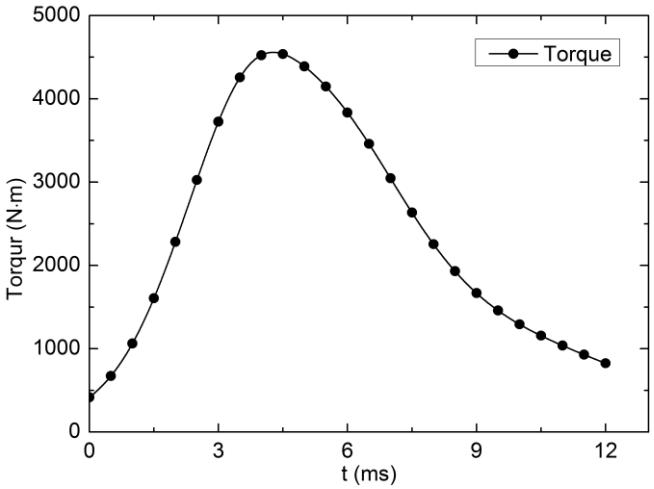

(c) Torque

Fig. 8 Curve of loading conditions

An outside force must be applied to drive the spinning of the projectile assembly with rifling not modeled. The torque-time curve used in this analysis is derived from the p-t curve. The relation between the torque and angular acceleration is

$$T=I\alpha \quad (1)$$

Where I is the polar moment of inertia. For the projectile is spin stabilized, the angular acceleration is proportional to the base acceleration derived from the pressure.

$$\alpha = Ka \tag{2}$$

Where K can be calculated using the following formula:

$$K = \tan\theta = \pi / \eta \tag{3}$$

Where η refers to the twist of rifling, θ is the angle between the circumferential twist distance and the axial distance.

Thus the torque can be calculated using the following formula:

$$T = \pi a I / \eta \tag{4}$$

The derived torque calculated from equation (4) applied to the band is shown in Fig.8 (c). The boundary condition of torque and base acceleration is shown in Fig.9. As it can be seen from Fig.8, the maximum base pressure is 404 MPa at 4.27 ms from ignition. The maximum acceleration and torque derived from the base pressure is 17953 G's and 4558 N• m respectively.

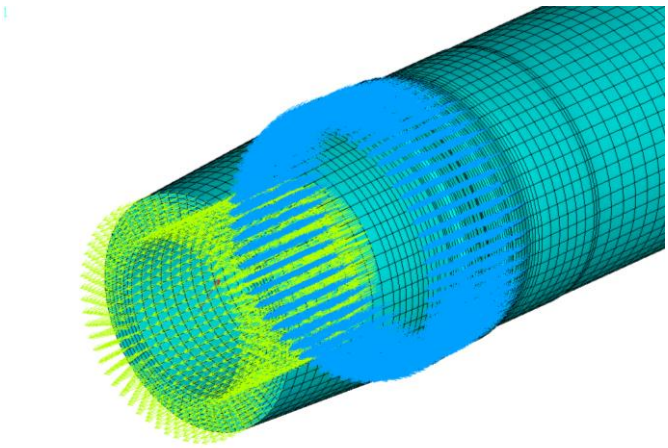

Fig. 9 Torque and base acceleration

D. *Contact type*

Interfacing between various contact surfaces within the isolator and projectile are defined by selecting a set of elements on each of the two contacting parts attached to the contact area. Then the contact type and the role acted by each part are introduced. Contact definitions among various parts of the model are summarized in Table II.

TABLE II CONTACT DEFINITION

Master	Slave	Contact type
breech	Gun tube	Tied surface to surface
Gun barrel	hollow steel shell	Automatic surface to surface
Gun barrel	band	Eroding surface to surface
hollow steel shell	housing	Tied surface to surface
housing	Bearing	Automatic surface to surface
shaft	Bearing	Tied surface to surface

Besides setting above, the simulating termination time is set 18 ms, while the remainder settings are defaulted.

IV. ANALYSIS APPROACH

A. *The gun barrel's deformation under gravity*

We can see the gun barrel at 52 degrees QE deformation from Fig.10. The deformed gun barrel under the gravity simulated in the implicit process would be imported to the process of explicit simulating as the initial conditions. It's easy to find that the gun muzzle's deformation is 2.032 mm in Fig.10.

B. *The displacement and velocity of the projectile*

It shows the velocity of projectile moving in the gun tube along the centerline (axial direction) in Fig. 11. The muzzle velocity occurred about 12 ms. It is easy to know the velocity reaches to 945 m/s from the curve. It approximates to the velocity in the living firings.

As mentioned above, the gravity was applied to the model in the x and y directions. The displacement curve of projectile in y direction tends to deviate from centerline with slightly fluctuation. Fig.12 reveals the displacement of the projectile during launch in x and y directions. From the curve, it is obvious to see the displacement in y direction of projectile exceeds 2 mm at the muzzle, which verifies the gun tube's deformation at 52 degrees quadrant elevation by implicit analysis.

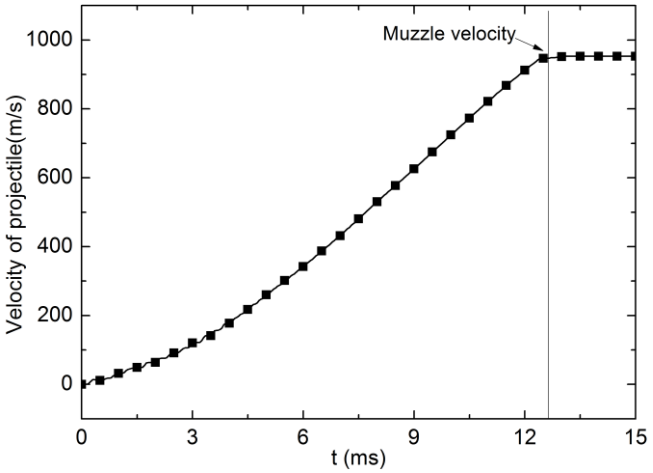

Fig. 11. Projectile velocity along centerline of gun tube

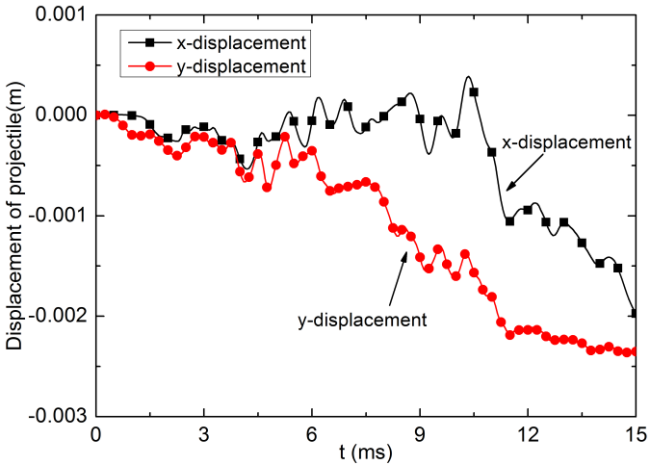

Fig. 12. Projectile displacement in x and y direction

C. The bearing's dynamic response

The bearings are regarded as the critical parts in the isolator; they realize the relative rotation between the projectile and the fixed canard. The bearing is sensitive to the shock loadings so that it is easy to be out of shape and crack in the process of launch. Therefore, we conduct an analysis for the dynamic response of the three bearings in the isolator shown in Fig.13 through implicit-explicit sequential simulation in the following sections.

There are two simplified ball bearings in isolator showed in Fig.13. They are comprised of the inner ring, outer ring and the rollers. It is obvious to see one ball bearing on the right side is smaller than the other one. It is labeled No.1.The bigger one on the left side is labeled No.2. Fig.14 shows the configuration of the No.1 ball bearing. The dynamic response of the two ball bearings and the thrust bearing under shock loadings are discussed as follows.

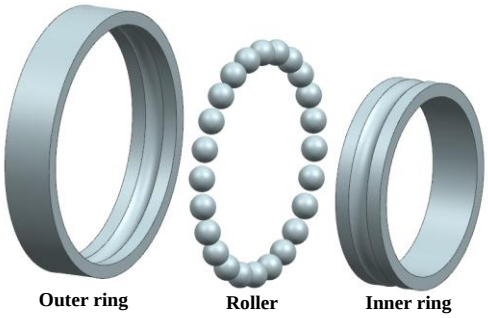

Fig. 14. No.1 ball bearing

We can see the axial acceleration's changing curve of the three parts in No.1 bearing during lunch from Fig.15, 16 and 17. As can be seen in the figure, the variation tendency of curves is similar to the change of base pressure. The axial acceleration of the outer ring, inner ring and roller reach to the maximum 20,800 G's synchronously. The maximum appears at about 4.3 ms. The fluctuate curves whose value is up to at least 10,000 G's at about 12 ms indicate the projectile vibrations when the axial force is removed. Therefore, the axial loading is mainly affected by such two factors as base pressure in the internal barrel and pressure dissipation at the muzzle exit.

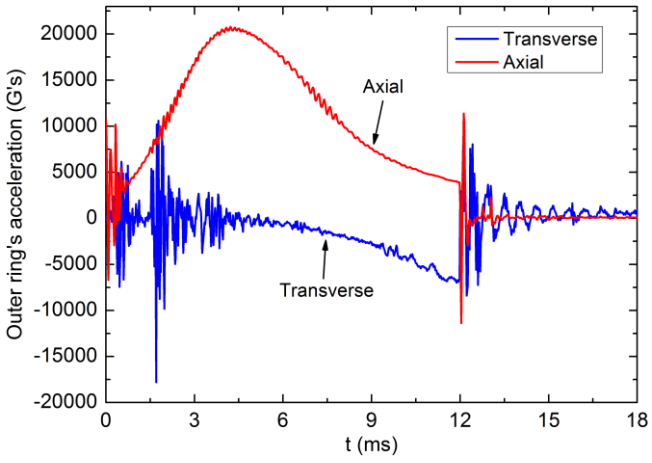

Fig. 15. Acceleration of No.1 ball bearing's outer ring

We also can see transverse acceleration's changing curve of the three parts in No.1 bearing in the process of projectile moving from Fig.15, 16 and 17. The graph describes that transverse load increases gradually when the projectile moves near the muzzle exit under the effect of the gun tube's deformation. It is similar with the axial acceleration. The fluctuation of curve at about 12 ms shows the transverse load's high frequency oscillation resulted from pressure dissipation. The transverse acceleration's numerical value of roller, outer ring and inner ring in No.1 bearing occurring at about 12 ms are 15,100 G's, 8,400 G's and 14,300 G's, respectively.

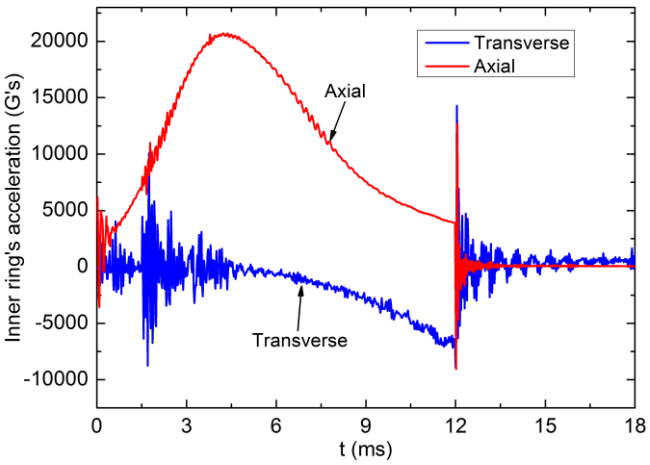

Fig. 16. Acceleration of No.1 ball bearing's inner ring

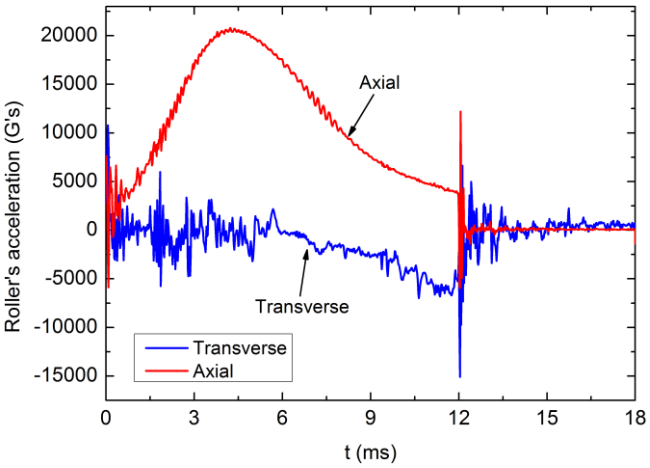

Fig. 17. Acceleration of No.1 ball bearing's roller

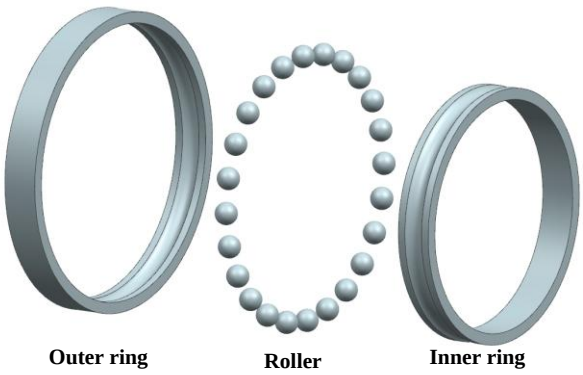

Fig. 18. No.2 ball bearing

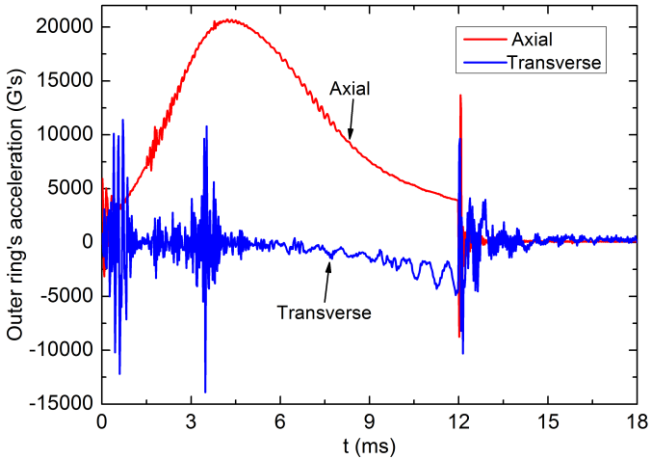

Fig. 19. Acceleration of No.2 ball bearing's outer ring

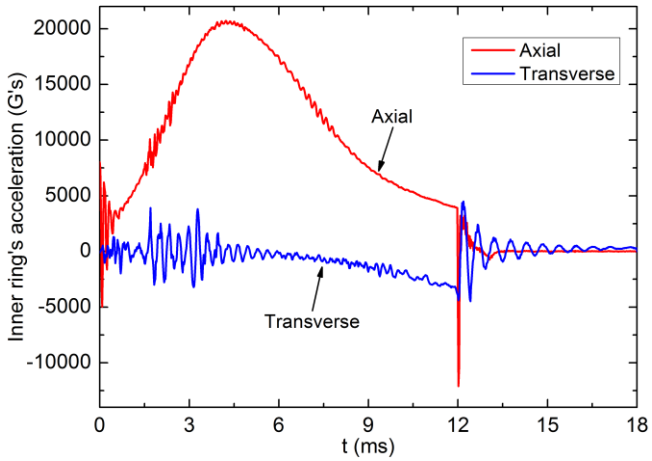

Fig. 20. Acceleration of No.2 ball bearing's inner ring

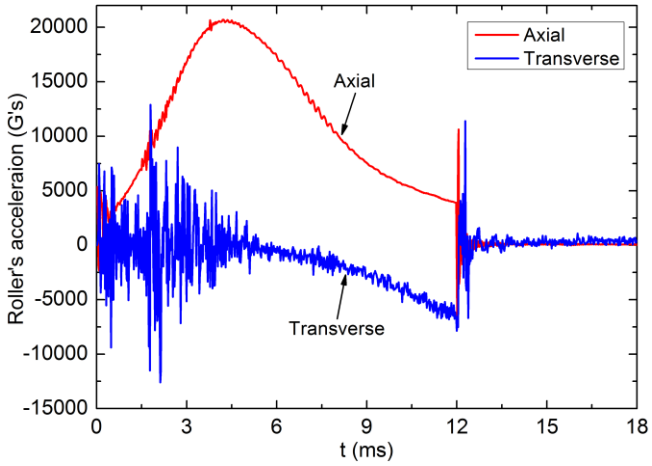

Fig. 21. Acceleration of No.2 ball bearing's roller

Similarly, it shows the simplified configuration of the No.2 bearing in Fig.18. It is obvious to see the change of the axial acceleration from the Fig.19, 20 and 21. It is similar with the No.1 bearing. The axial acceleration's maximum of roller, outer ring and inner ring reach to about 20,700 G's at about 4.4 ms. It also can be seen from Fig.19, 20 and 21 that the change of transverse acceleration of the three parts in No.2 bearing with projectile travelling in the tube. In addition to the curves' fluctuating at muzzle exit, the curves of roller and outer ring fluctuate sharply from ignition to 5 ms. The vibration amplitude of them are 12,900 G's and 13,900 G's, respectively. The accelerative spinning of projectile and violent impacts with the barrel inside wall may contribute to such high transverse shock.

As Fig.22 shows, the simplified thrust bearing is comprised of needle roller, cage, shaft washer and seat washer. The change of the thrust bearing's axial acceleration showed in Fig.23, 24 and 25 is identical with the trend of base pressure, whose maximum reach to 20,700 G's at about 4 ms. The thrust bearing's change of transverse acceleration is also described in Fig.23, 24 and 25. The transverse acceleration of needle roller reaches the top at 6.6 ms, not at the time that projectile moves out of the muzzle exit. The thrust bearing is tend to be more vulnerable than the ball bearings when it meets the transverse shock loadings, such as the centrifugal inertia force and gyroscopic couple produced by the accelerative spinning of projectile and violent impacts with the barrel inside wall. According to the boundary conditions, the base pressure can influence projectile's spin. Therefore, the transverse shock is affected by the factors such as the gun tube deformation, the spinning produced by the base pressure and the pressure dissipation at muzzle exit.

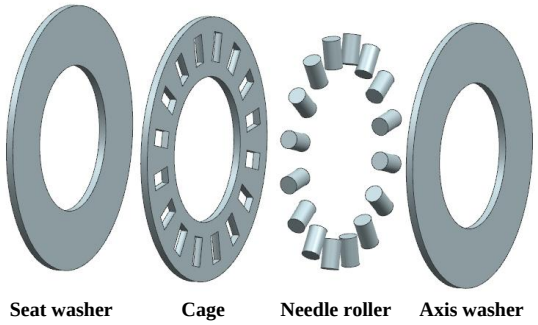

Fig. 22 The thrust bearing

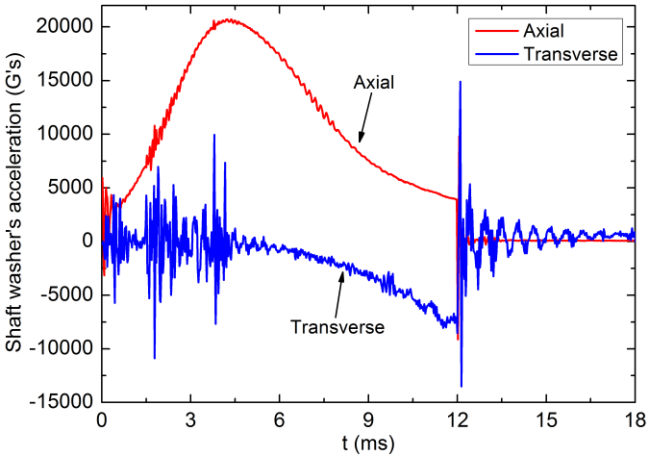

Fig. 23. Acceleration of thrust bearing's shaft washer

Based on the acceleration, the axial and transverse's applied force can be calculated if the mass of bearing has been given. Then, we will deduce a calculation method to obtain the maximum contact stress resulted from the maximum acceleration on the basis of Hertz theory.

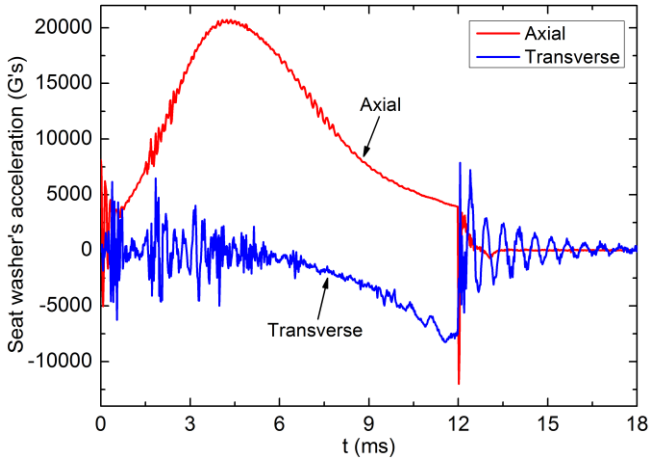

Fig. 24. Acceleration of thrust bearing's seat washer

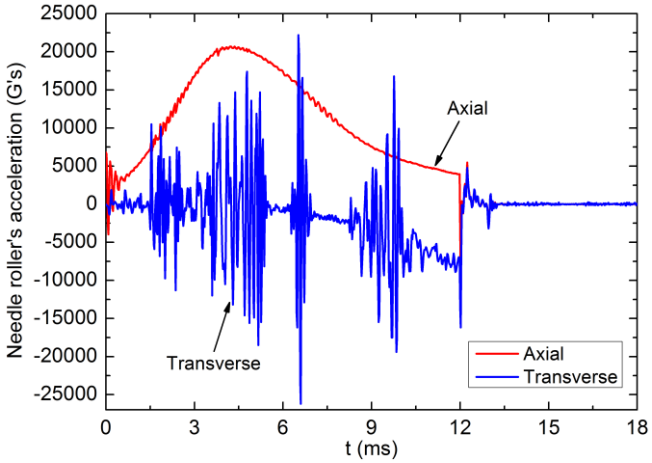

Fig. 25. Acceleration of thrust bearing's needle roller

D. Stress analysis

The maximum contact stress and deformation of bearing are affected by the parameters such as elasticity modulus, poisson's ratio, curvature sum $\sum\rho$, curvature difference $F(\rho)$ and load.

As mentioned in previous section, the bearings experienced combined the axial load F_a the transverse load F_t at any moment during the launch process. For the ball bearing whose contact angle α under this condition, $Q_{\max}$ should be calculated through the formula in the following:

$$Q_{\max}=\frac{F_a}{J_a Z\sin\alpha} \tag{5}$$

Where J_a is the thrust integral which is determined by the dimension of the ball bearing and Z is the number of the rolling elements. The thrust load F_a and the radial load F_t can be obtained through Newton's Law if the bearing's acceleration and mass have been known.

In this paper, the bearings are made of steel. Therefore, for the two ball bearings, the contact type is point contact, and the shape of the deformed surface is an ellipsoid of revolution. The maximum contact stress and deformation can be calculated based on the following formulas:

$$a=0.0236a^*\left(\frac{Q_{\max}}{\sum\rho}\right)^{1/3} \tag{6}$$

$$b=0.0236b^*\left(\frac{Q_{\max}}{\sum\rho}\right)^{1/3} \tag{7}$$

$$\delta=2.79\times10^{-4}\delta^* Q_{\max}^{2/3}\sum\rho^{1/3} \tag{8}$$

$$\sigma_{\max}=\frac{3Q_{\max}}{2\pi ab} \tag{9}$$

Where δ is the relative approach of remote points in the contacting bodies. a^* and b^* are the dimensionless semi-major axis of contact ellipse, and the dimensionless contact deformation δ^* are the function of curvature difference $F(\rho)$. a and b are the semi-major axis of the projected contact ellipse which are showed in Fig.26 and 27.

Different with the ball bearing, the contact type of thrust bearing is line contact, and the shape of the deformed surface is a semi-cylindrical form. For this condition, the maximum contact stress and deformation can be calculated based on the following formulas:

$$\sigma_{\max}=\frac{2Q_{\max}}{\pi lb} \tag{10}$$

$$b=3.35\times10^{-3}\left(\frac{Q_{\max}}{l\sum\rho}\right)^{1/2} \tag{11}$$

Where b is the semi-width of the contact surface showed in Fig. 28 and 29.

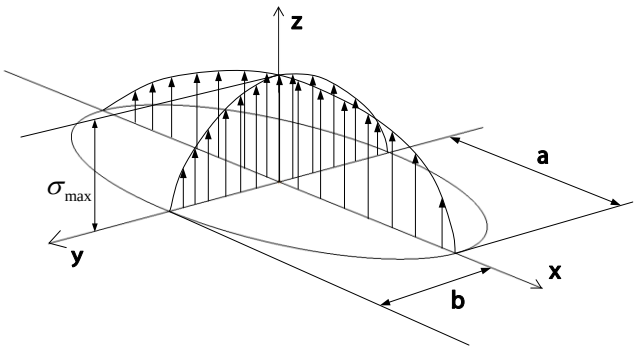

Fig. 26. Ellipsoidal surface compressive stress distribution of point contact of ball bearing

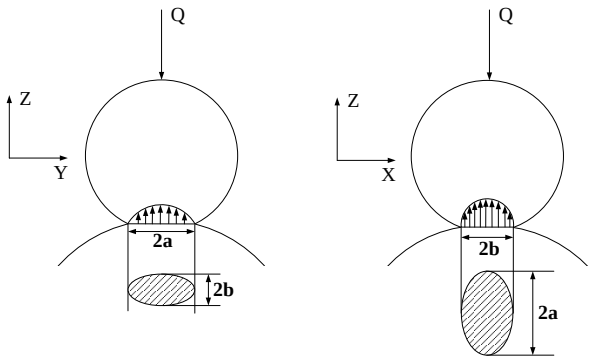

Fig. 27. Surface compressive stress distribution of point contact

Based on the analysis in Part C of Section IV, we can obtain the maximum acceleration of the two ball bearings and the thrust bearing in axial and transverse direction. However, it can be apparently seen that the maximum axial and transverse acceleration do not occur simultaneously. Thus, we calculate the maximum contact stress of the three bearings' components in the condition of the maximum acceleration in the axial and transverse direction, respectively. Table III, IV and V shows

the calculated maximum contact stress of the three bearings' components.

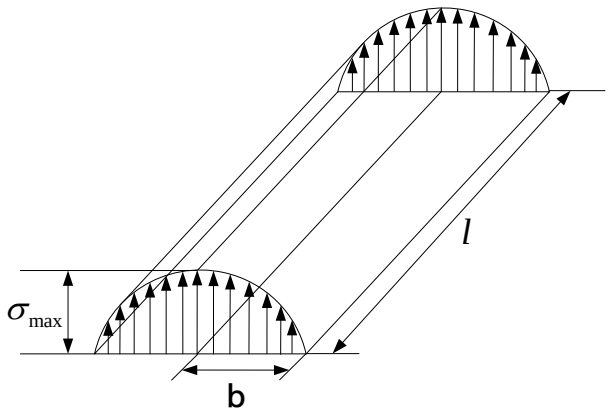

Fig. 28. Semi-cylindrical surface compressive stress distribution of line contact of thrust bearing

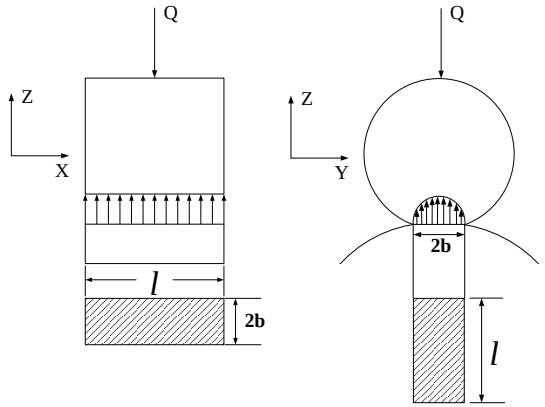

Fig. 29 Surface compressive stress distribution of line contact

Furthermore, we also acquired the maximum contact stress of the three bearings' components through simulation to compare the calculated results. It is obvious to see the contact stress time history which is about three bearings' components from Fig.30, 31 and 32. The simulation values of those components' contact stress are extracted from those figures and listed them in Table VI, VII and VIII.

It can be discovered from the data in Table III that stress of No.1 bearing's outer ring, inner ring and roller in the condition of maximum axial acceleration is larger than the stress when those are subjected to the maximum transverse acceleration. On the contrary, for the No.2 ball bearing, the stress under the condition of maximum transverse acceleration is larger than that under the maximum axial acceleration based on the data in Table IV. The results indicate that the contact stress of bearing is decided by the axial and transverse shock loadings together. For thrust bearing, from data in Table V it can be apparently illustrated that the axial shock loadings could be the main factor which decides the maximum contact stress of the thrust bearing. Although the thrust bearing is tend to be vulnerable to transverse shock loadings.

Compared with the calculation results extracted from Table III, IV and V and added in Table VI, VII and VIII, on the one hand, it can be seen that the moment of simulation results is relatively close to the calculation results. On the other hand, the calculated values maximum contact stress are relatively close to the simulation values. The calculation results and the simulation results are approximative. This verifies the validity and feasibility of the maximum contact stress's calculative method.

TABLE VI SIMULATION AND CALCULATION VALUES OF MAXIMUM CONTACT STRESS OF THE NO.1 BALL BEARING'S COMPONENTS

No.1 ball bearing		outer ring	inner ring	roller
simulation results	moment (ms)	4.66	5.05	5.2
	Maximum contact stress (MPa)	109	150	188
calculation results	moment (ms)	4.3	4.3	4.3
	Maximum contact stress (MPa)	104	145	177

TABLE VII SIMULATION AND CALCULATION VALUES OF MAXIMUM CONTACT STRESS OF THE NO.1 BALL BEARING'S COMPONENTS

No.2 ball bearing		outer ring	inner ring	roller
simulation results	moment (ms)	3.07	3.26	2.8
	Maximum contact stress (MPa)	409	511	693
calculation results	moment (ms)	3.48	3.27	2.2
	Maximum contact stress (MPa)	397	518	637

TABLE VIII SIMULATION AND CALCULATION VALUES OF MAXIMUM CONTACT STRESS OF THE THRUST BEARING'S COMPONENTS

thrust bearing		shaft washer	seat washer	needle roller
simulation results	moment (ms)	5.14	5.08	3.7
	Maximum contact tress (MPa)	483	522	1,102
calculation results	moment (ms)	4.36	4.56	3.9
	Maximum contact tress (MPa)	476	513	1,043

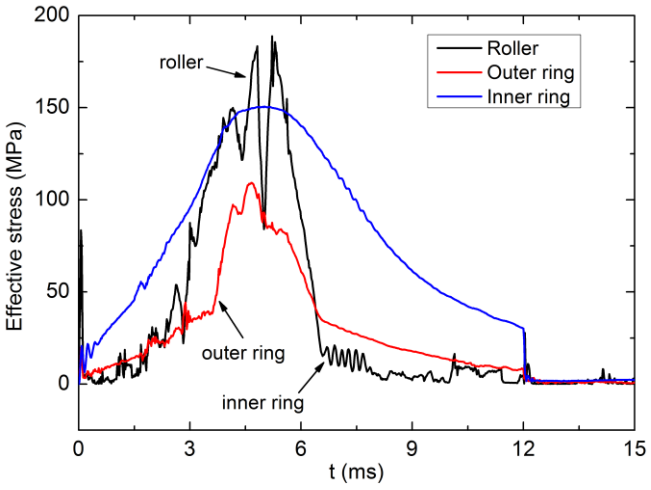

Fig.30. Simulation contact stress of No.1 ball bearing during launch process

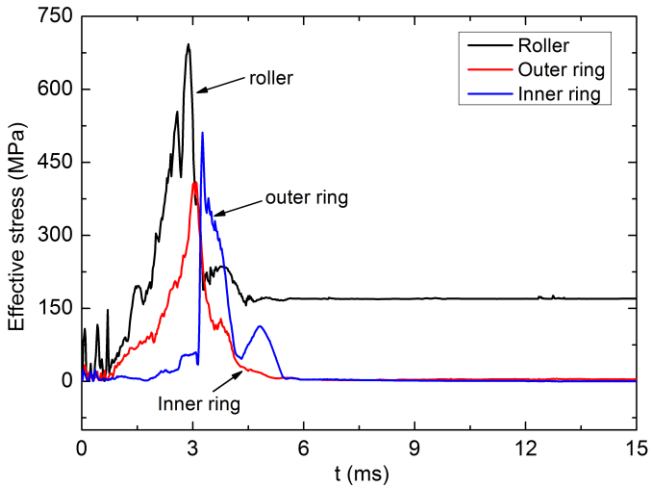

Fig.31. Simulation contact stress of No.2 ball bearing during launch process

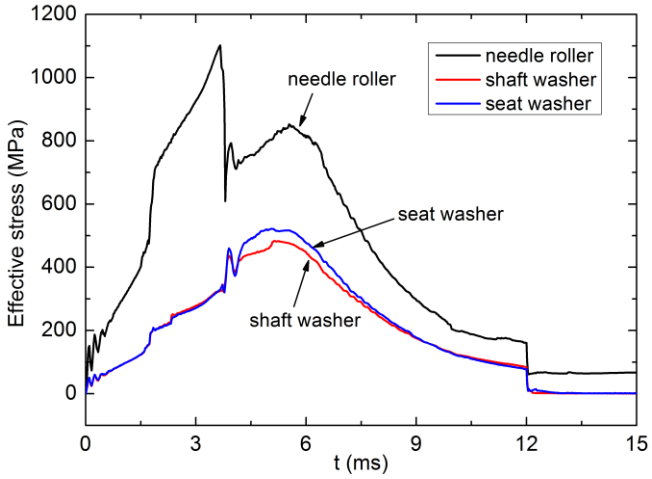

Fig.32. Simulation contact stress of thrust bearing during launch process

In addition, it is obvious to see that the bearings' deformation are within the scope of elasticity by comparing with the yield stress of bearing steel (quenched and tempered) in Table I. Therefore, the data results indicate that the two ball bearings and the thrust bearing can work well during flight after launch.

V. Conclusion

Course Correcting Fuse within a projectile is subjected to high shock loadings during launch. The researchers used the traditional method to oversimplify the model to study dynamic response of the components in ammunition under severe shock loadings. Beyond that, they also neglected the effect of gravity; gun tube's deformation and muzzle's pressure dissipation. Therefore, this paper presents a research method for shocks on the rotation isolator used in this fuse, which can realize the relative rotation between projectile and fuse. The researchers design a integrated model which includes the isolator, the projectile and gun tube.

With the help of the implicit-explicit sequential finite element dynamic analysis, we can obtain the displacement in x and y direction and the muzzle velocity and verify the gun tube's deformation under gravity. Then the dynamic response of bearings is described. It can be concluded that the base pressure is the key factor to affect the axial maximum loads applied on the fuse. The gun tube's deformation under gravity, base pressure and pressure dissipation which result in the fluctuating transverse shock loadings cannot be neglected. Besides, due to the projectile's accelerative spin and violent collision with the barrel's inside wall, the transverse shock loadings is tend to be influenced by centrifugal inertia force and gyroscopic couple. The research results can be useful for reducing chances for the fuse's failure during launch..

According to the acceleration acquired by simulation, a calculation method is proposed to work out the maximum contact stress of the bearing's components. The method is combined with the bearing's maximal contact stress in the process of simulation. The results verify the calculation method's validity and applicability by comparing the numerical value of the bearing's maximal contact stress. Besides, the results indicate that bearings can operate normally during launch. This kind of structure design of rotation isolator used in the fuse can be a reference for engineers' research about the loading equipment.

References

[1] T. E. Simkins, G. A. Pflegl, and E. G. Stilson, "Dynamic strains in a 60MM gun tube: an experimental study," *Journal of Sound Vibration*, vol. 168, 1993, pp.549-557.

[2] M. S. L. Hollis, "Use of finite-element stress analysis in the design of a tank-cannon- launched training projectile," *Report for the Department of Army*, Report no. ARL-MR-149, September 1994.

[3] D. A. Hopkins, Wilkerson SA. "Analysis of a balanced breech system for the M1A1 main gun system using finite element techniques," *Report for the Department of Army*, Report no. ARL-TR-608, November 1994.

[4] D. E. Carlucci, J. Cordes, J. Hahn, et al, "Electronics and the gun environment," *Ferroelectrics*, vol.342, 2006, pp.193–204.

[5] B. R. Sorenson, "Design and analysis of Kinetic energy projectile using Finite-Element Optimization," Report for the Department of Army. Report no. BRL-TR-3289, November 1991.

[6] G. M. Heaslip, J. M. Punch, "Analysis of experimental shock and impact response data of a printed wire board," *2003 ASME International Mechanical Engineering Congress*, Washington D. C., 2003.

[7] S. S. Kessler, S.M. Spearing, "Design, analysis and Tesing of a high-g composite fuselage structure," *Proceedings of the American society of composite*, Dayton, 2000.

[8] M. R. Chowdhury, A. Frydman, J. S. Corde, et al. "3-D Finite-element gun launch simulation of a surrogate Excalibur 155 mm guided artillery projectile-modeling capabilities and its implications," *22nd International Symposium on Ballistics*, Vancouver BC, 2005.

[9] E. Petersen, "AGS barrel motion during firing: experimental and modeling results," *Proceedings of the 2005 SEM annual conference and exposition on experimental and applied mechanics*, Bethel, 2005.

[10] V. Chakka, M. B. Trabia, B. J. O'Toole, et al, "Modeling and reduction of shocks one electronic components within a projectile," *International Journal of Impact Engineering*, vol. 35, 2008, pp.1326-1338.

[11] J. T. Tzeng, W. Sun, "Dynamic response of cantilevered rail guns attributed to projectile/gun interaction-theory," *IEEE Transaction on Magnetics*, vol. 43, 2007, pp.207-213.

[12] K. D. Laughlin, "Characterization of the parameters that affect projectile balloting using finite element analysis," Ph.D. Thesis, University of Oklahoma, 2008.

[13] D. S. Somasundaram, "Experimental investigation of shock mitigation of electronic boards within projectiles," M. S. Thesis, University of Nevada, 2008.

[14] L. E. Reinhardt, J. A. Cordes, A. S. Haynes, et al. "Assessment of Need for Solder in Modeling Potted Electronics During Gun-Shot," *International Journal of Applied Mechanics*, vol. 80, 2013, pp.031502.

[15] X. W. Yin, P. Verberne and S. A. Meguid, "Multiphysics modeling of the coupled behavior of precision-guided projectiles subjected to intense shock loadings," I*nternational Journal of Mechanics and Materials in Design*, vol. 10, 2014, pp.439-450.

[16] S. J. ValderRade, D. A. Inman, and J. Daniel, "Using passive techniques for vibration damping in mechanical systems," *Journal of the Brazilian Society of Mechanical Sciences and Engineering*, vol. 22, 2000, pp.411-421.

[17] S. Sueki, S. G. Ladkany and B. J. O'Toole, "Experimental and computational study of acceleration response in layered cylindrical structure considering impedance mismatch effect," *Shock and Vibration*, vol. 18, 2011, pp.807-826.
[18] D. Carlucci, J. Cordes, S. Morris, et al. "Muzzle Exit (Set Forward) Effects on Projectile Dynamics," *Report for the Department of Army*, Report no. ARAET-TR-06003, 2006.
[19] M. Berman, D. Hopkins, D. Powers, et al. "Numerical and Experimental Modeling of the Transition from Transient to Quasi-static Loading of Printed Wiring Assemblies," *2003 SEM Annual Conference and Exposition on Experimental and Applied Mechanics*, Charlotte, 2003.
[20] J. A. Cordes, J. Vega, D. E. Carlucci, et al. "Structural loading statistics of live gun firings for the army's Excalibur projectile," *Report for the Department of Army*, Report no. ARAET-TR- 05005, 2005.
[21] S. Cui, X. Li, S. Wu, et al. "Anti-shock analysis of the electromagnetic launched projectile powered by the pulsed alternator," *19th IEEE International Pulsed Power Conference, San Francisco*, 2013.
[22] M. M. Chen, "Projectile balloting attributable to gun tube curvature," *Shock and Vibration*, vol.17, 2010, pp. 39-53.
[23] K. Kuncham, "Shock effects on electronic components within a projectile," M.S. Thesis, University of Nevada, 2006.
[24] J. A. Cordes, J. Lee, T. L. Myers, "Statistical Comparisons Between Qualification Tests for Gun-Fired Projectiles," *Journal of Applied Mechanics*, vol.77, 2010, pp. 051602

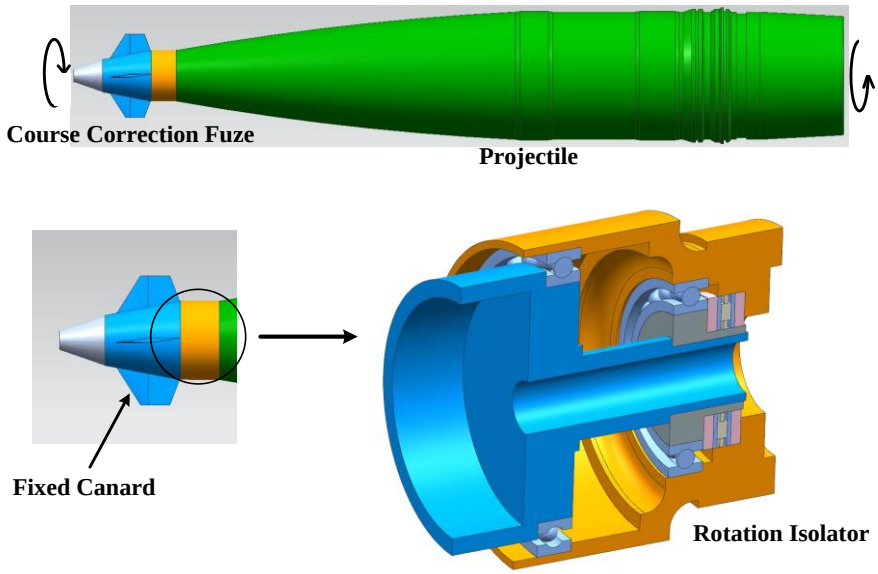

Fig. 2. Rotation isolator in the Course Correcting Fuse

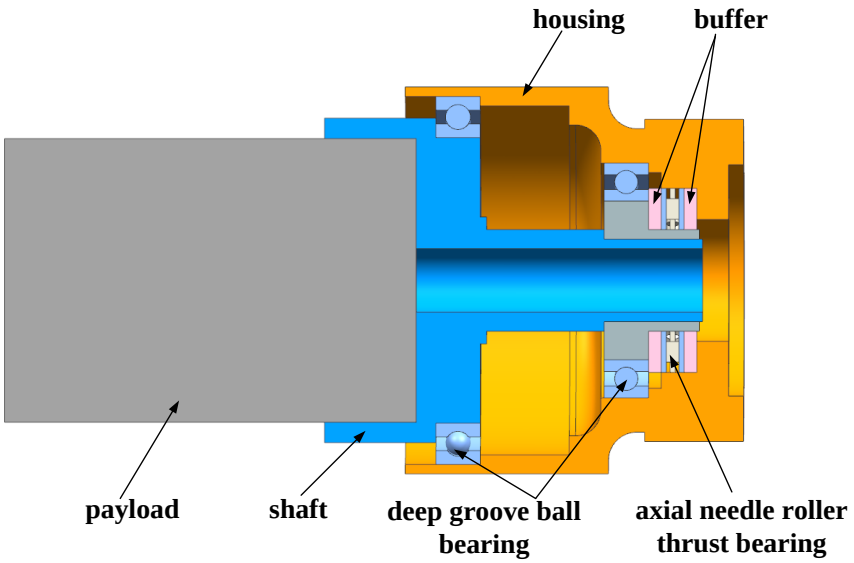

Fig. 3. Sectional view of the rotation isolator

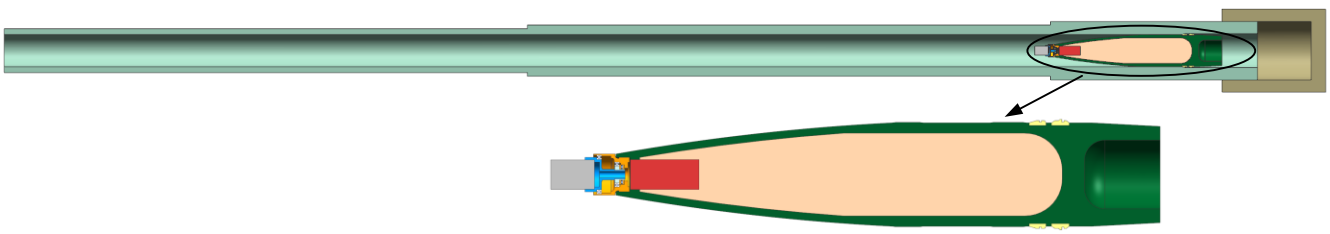

Fig. 4. Sectional view of gun tube and projectile with isolator

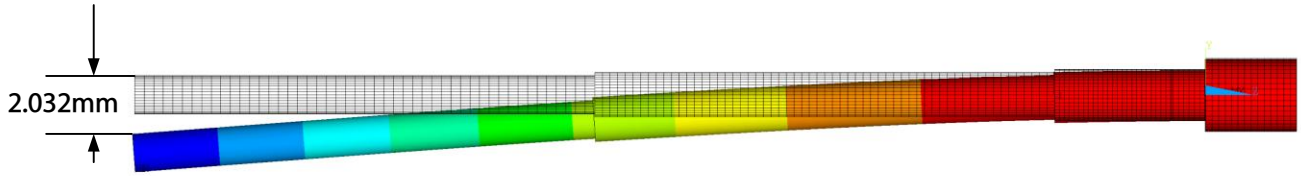

Fig. 10. Gun barrel's deformation due to gravity at 52 degrees quadrant elevation

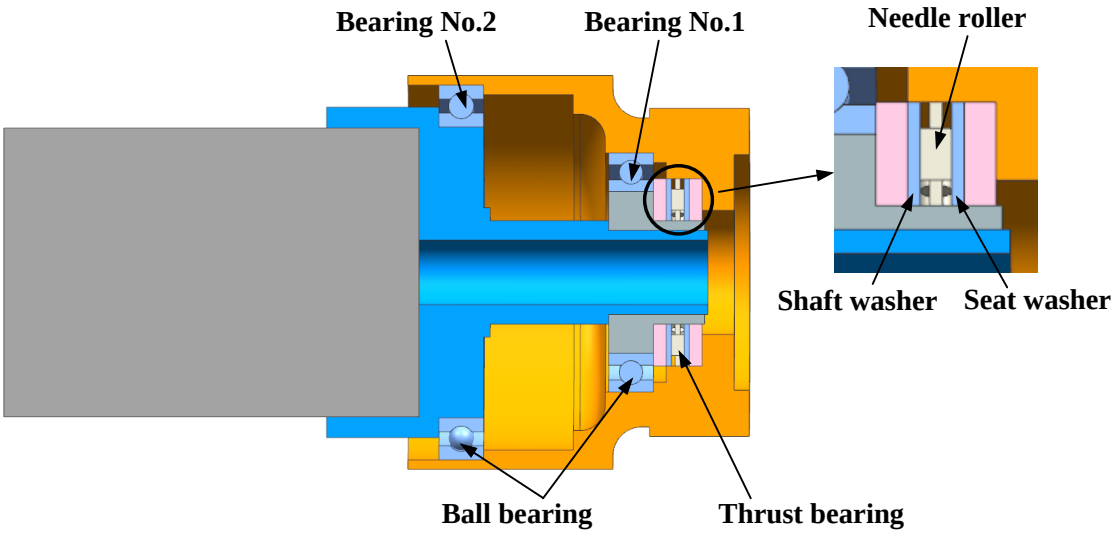

Fig. 13. Bearings in the isolator

TABLE I MATERIAL PROPERTIES AND CHARACTERISTICS OF MODEL

Part name	Material	Young's modulus (GPa)	Poisson's ratio	Yield stress (MPa)
gun tube breech	Alloy steel	380	0.32	1104
band	Red copper	125	0.34	206
hollow steel shell	4030 steel	210	0.29	510
charge	TNT	4.13	0.40	———
housing shaft	Aluminum alloy	71	0.33	280
bearing	Bearing steel (quenched and tempered)	219	0.30	1668

TABLE III CALCULATED VALUE OF MAXIMUM CONTACT STRESS OF NO.1 BALL BEARING

No.1 ball bearing	outer ring		inner ring		roller	
state	axial maximum	transverse maximum	axial maximum	transverse maximum	axial maximum	transverse maximum
moment (ms)	4.3	1.7	4.3	12.04	4.3	12.04
axial acceleration (G's)	20800	8690	20800	9680	20,800	5,950
transverse acceleration (G's)	680	17800	848	14300	567	15,100
contact stress (MPa)	104 (maximum)	61	145 (maximum)	15	177 (maximum)	105

TABLE IV CALCULATED VALUE OF MAXIMUM CONTACT STRESS OF NO.2 BALL BEARING

No.2 ball bearing	outer ring		inner ring		roller	
state	axial maximum	transverse maximum	axial maximum	transverse maximum	axial maximum	transverse maximum
moment (ms)	4.4	3.48	4.4	3.27	4.4	2.2
axial acceleration (G's)	20712	19109	20720	18523	20,710	10,692
transverse acceleration (G's)	154	13900	215	4120	1,250	12,900
contact stress (MPa)	191	397 (maximum)	409	518 (maximum)	167	637 (maximum)

TABLE V CALCULATED VALUE OF MAXIMUM CONTACT STRESS OF THRUST BEARING

thrust bearing	shaft washer		seat washer		needle roller	
state	axial maximum	transverse maximum	axial maximum	transverse maximum	axial maximum	transverse maximum
moment (ms)	4.36	12.1	4,56	12.4	3.9	6.6
axial acceleration (G's)	20700	4880	20700	1380	20,700	15,400
transverse acceleration (G's)	1690	14900	1390	7220	6010	26,200
contact stress (MPa)	476 (maximum)	19	513 (maximum)	9	1043 (maximum)	30